Available online at www.sciencedirect.com

ScienceDirect

*Mendeleev Commun.*, 2024, **34**, 664–666

Mendeleev Communications

# Lead sulfide quantum dots in an organic solar cell active layer

**Jorge Cruz-Gómez,[a] Francisco Javier de Moure-Flores,[a] Sandra Andrea Mayén-Hernández,[a] José Guadalupe Quiñones-Galván,[b] Aruna Devi Rasu Chettiar,[a] Claudia Elena Pérez-García[a] and José Santos-Cruz*[a]**

[a] *Facultad de Química, Posgrado en Energía, Universidad Autónoma de Querétaro, Querétaro, Qro., CP 76010, México. E-mail: jsantos@uaq.edu.mx*

[b] *Departamento de Física, Centro Universitario de Ciencias Exactas e Ingenierías, Universidad de Guadalajara, Guadalajara, Jal., CP 45129, México*

DOI: 10.1016/j.mencom.2024.09.012

**Organic solar cells have been fabricated using various concentrations of lead sulfide quantum dots. Data from Mott–Schottky analysis revealed intriguing changes in the bulk heterojunction layer of the solar cells that were directly related to the addition of the quantum dots. Notably, the highest power conversion efficiency of 5.15% was achieved with the addition of 0.4 wt% lead sulfide quantum dots.**

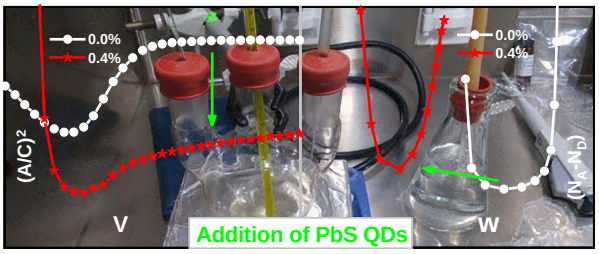


*Keywords*: organic solar cells, PbS quantum dots, PTB7, ligand exchange, Mott–Schottky.

Quantum dots (QDs) have drawn significant attention as a material for organic solar cells (OSCs) due to their properties of high mobility, tunable bandgap, solution processibility, dispersibility and applicability to large areas.[1] The lead sulfide quantum dots (PbS QDs) have been extensively investigated by several research groups due to their excellent optical properties.[2] Indium-doped tin oxide (ITO) substrate is typically used to fabricate OSCs, which increases their fabrication cost and makes them not adequate for commercialization.[3] Therefore, we replaced ITO with fluorine-doped tin oxide (FTO). In the fabrication process of OSCs, PbS QDs are first synthesized using oleic acid, and a ligand exchange process is conducted to employ PbS QDs efficiently in OSCs. Then, different concentrations of PbS QDs from 0.1 to 5.3 wt% are incorporated into poly({4,8-bis[(2-ethylhexyl)oxy]benzo[1,2-*b*:4,5-*b*′]dithiophene-2,6-diyl}-{3-fluoro-2-[(2-ethylhexyloxy)carbonyl]thieno[3,4-*b*]-thiophene-4,6-diyl}) (PTB7) and fullerene derivative [6,6]-phenyl-$C_{71}$-butyric acid methyl ester (PC70BM) to use as the active layer in OSCs. Besides, reference OSCs are fabricated without PbS QDs. Moreover, the highest power conversion efficiency (PCE) of 5.15% is achieved with 0.4 wt% PbS QDs.[†]

Figure 1 shows the UV-VIS-NIR absorption spectrum of PbS QDs dissolved in toluene. The first absorption band is at 1218 nm. Using the Tauc method, the bandgap was estimated to be 0.96 eV.[5] Using the empirical relationship [equation (1)] reported by Wei *et al.*,[6] the average diameter $D$ of the QDs was estimated to be 4.6 nm:

$$D = \{0.85 + [0.7225 + 3.84(1243/\lambda - 0.41)]^{1/2}\}/(1243/\lambda - 0.41), \quad (1)$$

where $\lambda$ is the wavelength (in nm) of the first absorption band of PbS QDs, and $D$ is the diameter (in nm).

PbS QDs of this size were used due to the width of their bandgap and the values of their energy levels of the valence and conduction bands. Using the method from the work of Jasieniak

[†] Lead oxide (PbO, 99%, Meyer), oleic acid ($C_{18}H_{34}O_2$, reactive grade, Meyer), chlorobenzene (CB, 98%, Meyer), bis(trimethylsilyl) sulfide ($C_6H_{18}SSi_2$, 98%, Beantown Chemical), 1-octadecene ($C_{18}H_{36}$, 90%, GFS Chemicals), 1,2-ethanedithiol (EDT, $C_2H_6S_2$, 98%, Sigma-Aldrich), methanol, acetone, toluene, PC70BM (1-Material), poly[{9,9-bis[3-(dimethylamino)propyl]-9*H*-fluorene-2,7-diyl}-*alt*-(9,9-dioctyl-9*H*-fluorene-2,7-diyl)] (PFN, Solaris), 1,8-diiodooctane (DIO, 95%, Sigma-Aldrich), molybdenum trioxide ($MoO_3$, 99.5%, Sigma-Aldrich), FTO (Pilkington, thickness 500 nm, resistivity 25 to 30 Ω/□), PTB7 (Solaris, High MW) and aluminum (Ted Pella, 99.99%) were used as received, without additional treatment.

The protocol for the synthesis of PbS QDs by Hines and Scholes[4] was slightly modified.

For ligand exchange, EDT was added to the toluene solution of PbS QDs at a toluene/EDT volume ratio of 4 : 1 and stirred for 12 h at 70 °C and 24 h at room temperature. Afterwards, the QDs were washed. Finally, the PbS QDs were dissolved in a solvent mixture of CB and EDT (9 : 1, v/v) at a concentration of 25 mg $ml^{-1}$. Then, the PbS QDs were spin-coated onto FTO and Corning glass.

To fabricate solar cells, a solution of PFN (2 mg $ml^{-1}$) in methanol with acetic acid was spin-coated onto FTO to obtain a layer ~10 nm thick and annealed at 145 °C. Afterwards, the reference active layer was deposited using a solution of PTB7 and PC70BM (1 : 1.5, w/w) in CB with 3% DIO. Furthermore, the active layers were deposited using different concentrations of PbS QDs (0.1, 0.2, 0.3, 0.4, 0.6, 2.3 and 5.3 wt%). Finally, 15 nm of $MoO_3$ and 100 nm of Al were deposited using the physical vapor deposition technique.

Ultraviolet-visible-near-IR (UV-VIS-NIR) absorption spectrum was recorded using an Agilent Cary 5000 UV-VIS-NIR spectrophotometer. Transmission electron microscopy (TEM) and high-resolution TEM (HRTEM) images were acquired using JEOL instruments, JEM-1010 and JEM 2010F, respectively. Raman measurements were done using a Thermo Scientific DXR2 Raman microscope. Current density *vs.* voltage measurements were performed using an Oriel Instruments LCS-100 solar simulator. Thickness measurements were carried out using a KLA Tenkor D-100 profilometer. Electrical properties were determined using an Ecopia HMS-3000 Hall measurement system. Mott–Schottky data were obtained using a GAMRY 1000 potentiostat.

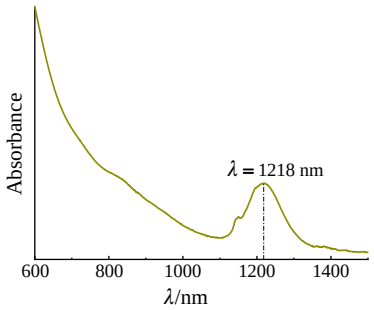


**Figure 1** UV-VIS-NIR absorption spectrum of 4.5 nm PbS QDs dissolved in toluene.

*et al.*,[7] the values of the energy levels of the conduction and valence bands were found, which were −4.04 and −5.00 eV, respectively. The conduction level is lower than that corresponding to PTB7 (−3.6 eV), but higher than the lowest unoccupied molecular orbital (LUMO) of PC70BM (−4.3 eV). This structure of energy levels in the PbS QDs is suitable for the absorption of photons in the infrared range with the possibility of forming multiexcitons with high energy photons (in the UV) and promotes the separation of excitons so that electrons remain in the LUMO of PC70BM and holes remain in the valence band of PbS QDs and on the highest occupied molecular orbital of PTB7. The cell generates a beneficial electrical potential when electrons are collected in the FTO through the LUMO of PFN, and holes are collected in the aluminum electrode through the $MoO_3$ conduction band.

Figure 2(*a*) displays the TEM image of PbS QDs. Based on the image, the QDs appear to be circular or ellipsoidal in shape. Figure 2(*b*) shows the size distribution histogram of the PbS QDs. The average size was 4.4 nm, which is close to the estimated one (4.6 nm). Figure 2(*c*) shows the HRTEM image of PbS QDs. From the image, interplanar distances of 0.34, 0.30 and 0.20 nm were obtained using the Image J software, corresponding to the (111), (200) and (220) planes, respectively, and these distances were close to the reported values of the standard powder material (PDF no. 05-0592). Figure 2(*d*) shows the selected area electron diffraction (SAED) pattern. In this pattern, diffraction rings from the (111), (200) and (220) planes were observed, which are characterized by the most significant interplanar distances and the highest relative intensities of 84, 100 and 57, respectively.[8] The results revealed that PbS QDs have different crystal orientations, and the higher the diffraction intensity from the crystalline planes, the larger the interplanar distance.

Figure 3(*a*) shows the Raman spectrum of PbS QDs. The modes are observed at 145, 207, 237 and 280 $cm^{-1}$. The vibrational mode at 145 $cm^{-1}$ is associated with the photooxidation

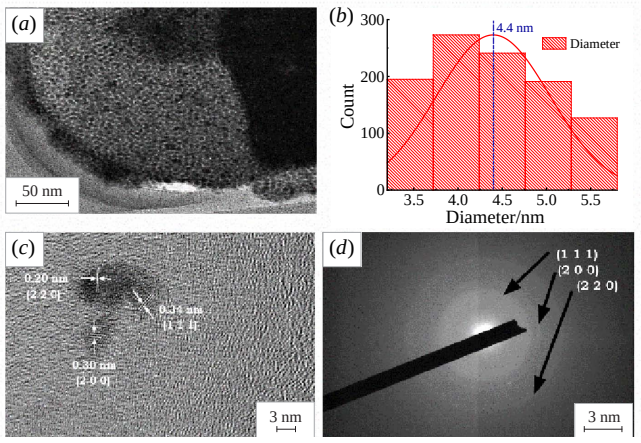


**Figure 2** (*a*) TEM image, (*b*) size distribution histogram, (*c*) HRTEM image and (*d*) SAED pattern of PbS QDs.

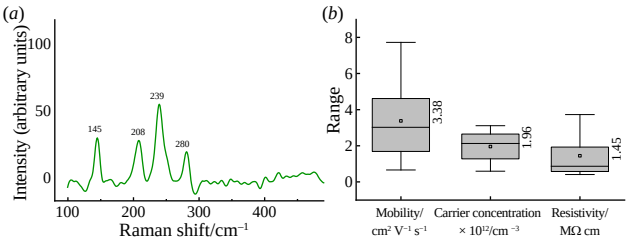


**Figure 3** (*a*) Raman spectrum of PbS QDs deposited on FTO obtained using a 532 nm laser. (*b*) Box diagram of the electrical properties of PbS films.

of PbS QDs due to laser energy.[9] The vibrational modes observed at 132 and 144 $cm^{-1}$ are ascribed to the stretching of Pb–O–Pb bonds.[10] The signal detected at 208 $cm^{-1}$ revealed the optical mode of the angular momentum $l = 0$ of the crystal lattice.[11,12] The vibrational mode at 280 $cm^{-1}$ is related to the presence of an optical phonon on the surface of PbS QDs due to the agglomeration during film deposition using an EDT binder;[9,13] the signal obtained at 239 $cm^{-1}$ corresponds to the substrate.[14]

Figure 3(*b*) shows the standard deviation of the electrical properties of PbS films from the Hall effect. The obtained resistivity values are consistent with those reported for inorganic semiconducting materials, whereas the carrier concentration values are lower than the reported values.[15]

Figure 4(*a*),(*b*) shows the average and maximum values of PCE and fill factor (FF), respectively, for different concentrations of PbS QDs. The maximum PCE and FF values were obtained for a concentration of 0.4 wt%. Figure 4(*c*) shows that the series resistance reached a minimum at 0.3 wt% and gradually increased at lower or higher concentrations of PbS QDs. The maximum parallel resistance [see Figure 4(*c*)] was observed at 0.4 wt% and decreased abruptly at higher or lower concentrations of PbS QDs. Although the series resistance does not show the minimum value at 0.4 wt%, this is compensated by the difference with parallel resistance, resulting in the highest efficiency at 0.4 wt% QDs. Comparing these values with cells manufactured using ITO is problematic since a proper comparison requires a cell that is the same in everything except the conductive oxide. Similar works were found, although different. The results found range from 6.2 to 12.8% PCE.[16–18] It should be noted that a direct comparison is not possible, given that there is a difference between the work functions of these materials, 4.7 and 5.0 eV for FTO and ITO, respectively. So, a cell structure that works using ITO does not work, or at least not as efficiently, with FTO, and *vice versa*.

Figure 5(*a*),(*b*) shows the notable difference between solar cells with PbS QDs and the reference solar cell. The addition of PbS QDs resulted in three changes in the bulk heterojunction

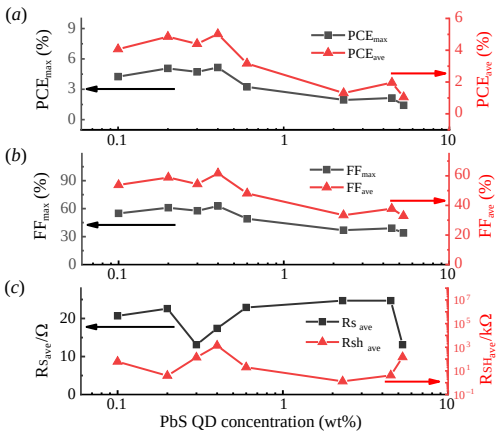


**Figure 4** Maximum and average values of (*a*) PCE, (*b*) FF and (*c*) series and parallel resistances of OSCs as a function of the concentration of PbS QDs added to the active layer.

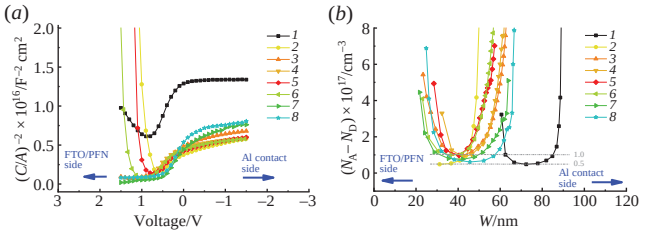


**Figure 5** Mott–Schottky plots of (*a*) the inverse square of capacitance per unit area $[(C/A)^{-2}]$ *vs.* applied voltage and (*b*) the difference between the concentration of p-type acceptor impurities and the concentration of n-type donor impurities ($N_A - N_D$) *vs.* the width ($W$) of the space charge region for solar cells made with the addition of (*1*) 0, (*2*) 0.1, (*3*) 0.2, (*4*) 0.3, (*5*) 0.4, (*6*) 0.6, (*7*) 2.3 and (*8*) 5.3 wt% PbS QDs.

(BHJ) layer: first, the concentration of acceptor impurities increased from $0.5 \times 10^{17}$ to $1.0 \times 10^{17}$ $cm^{-3}$ [Figure 5(*b*)]; second, the space charge region moved from the surface to the center of the BHJ layer [see Figure 5(*b*)]; and third, the capacitance of the p–n junction increased [Figure 5(*a*)]. Incorporation of PbS QDs into the BHJ layer changed the width of the space charge region [see Figure 5(*b*)]; the change depends on the added PbS QDs, the minimum of which was at 0.4 wt%. A similar change is observed in the concentration of acceptor impurities, which changed from $0.5 \times 10^{17}$ to $1.0 \times 10^{17}$ $cm^{-3}$, with the maximum again being at 0.4 wt% PbS QDs.

In conclusion, PbS QDs exhibited an average size of 4.4 nm and a bandgap of 0.96 eV. PbS QDs caused three changes in the BHJ layer: first, they increased the concentration of acceptor impurities from $0.5 \times 10^{17}$ to $1.0 \times 10^{17}$ $cm^{-3}$, second, they moved the space charge region from the surface of the BHJ layer to the center of the BHJ layer, and, third, they increased the capacitance of the p–n junction. Subsequently, a reference solar cell without PbS QDs was fabricated. Moreover, organic solar cells were fabricated by replacing ITO with FTO, and the best PCE value of 5.15% was obtained at 0.4 wt% PbS QDs, which is 3.6% higher than the reference solar cell.

We acknowledge the ‘Química Somos Todos’ fund for student projects 2021 (FQST21-FOPES) of the Faculty of Chemistry of the Autonomous University Querétaro. We also acknowledge the ‘Química Somos Todos’ fund to promote research consolidated modality 2021 (FQST21-FOMIC) of the Faculty of Chemistry of the Autonomous University Querétaro.

## References

1 M. Nam, *Org. Electron.*, 2021, **93**, 106150; https://doi.org/10.1016/j.orgel.2021.106150.
2 F. Qiao and Y. Xie, *J. Energy Chem.*, 2020, **48**, 29; https://doi.org/10.1016/j.jechem.2019.12.022.
3 J. Cruz-Gómez, G. I. García-Alvarado, M. Pal, S. A. Mayén-Hernández, F. De Moure-Flores, A. Sosa-Domínguez, R. Aruna-Devi and J. Santos-Cruz, *Optik*, 2021, **247**, 167961; https://doi.org/10.1016/j.ijleo.2021.167961.
4 M. A. Hines and G. D. Scholes, *Adv. Mater.*, 2003, **15**, 1844; https://doi.org/10.1002/adma.200305395.
5 B. D. Viezbicke, S. Patel, B. E. Davis and D. P. Birnie, III, *Phys. Status Solidi B*, 2015, **252**, 1700; https://doi.org/10.1002/pssb.201552007.
6 Y. Wei, M. Xing, D. Wang and R. Wang, *Energy Reports*, 2020, **6**, 2370; https://doi.org/10.1016/j.egyr.2020.08.033.
7 J. Jasieniak, M. Califano and S. E. Watkins, *ACS Nano*, 2011, **5**, 5888; https://doi.org/10.1021/nn201681s.
8 W. Meng, W. Yuan, Z. Wu, X. Wang, W. Xu, L. Wang, Q. Zhang, C. Zhang, J. Wang and Q. Song, *Powder Technol.*, 2019, **347**, 130; https://doi.org/10.1016/j.powtec.2019.02.035.
9 D. F. Garcia-Gutierrez, L. P. Hernandez-Casillas, M. V. Cappellari, F. Fungo, E. Martínez-Guerra and D. I. García-Gutiérrez, *ACS Omega*, 2018, **3**, 393; https://doi.org/10.1021/acsomega.7b01451.
10 J. L. Blackburn, H. Chappell, J. M. Luther, A. J. Nozik and J. C. Johnson, *J. Phys. Chem. Lett.*, 2011, **2**, 599; https://doi.org/10.1021/jz2000326.
11 R. Zhou, H. Niu, F. Ji, L. Wan, X. Mao, H. Guo, J. Xu and G. Cao, *J. Power Sources*, 2016, **333**, 107; https://doi.org/10.1016/j.jpowsour.2016.09.160.
12 M. Cheraghizade, R. Yousefi, F. Jamali-Sheini and A. Sa’aedi, *Majlesi Journal of Telecommunication Devices*, 2013, **2**, 163; https://sanad.iau.ir/Journal/mjtd/Article/901659.
13 M. Shkir, S. AlFaify, V. Ganesh and I. S. Yahia, *Solid State Sci.*, 2017, **70**, 81; https://doi.org/10.1016/j.solidstatesciences.2017.06.006.
14 X. Xia, W. Wu, Z. Wang, Y. Bao, Z. Huang and Y. Gao, *Sens. Actuators, B*, 2016, **234**, 192; https://doi.org/10.1016/j.snb.2016.04.110.
15 A. Goetzberger, J. Knobloch and B. Voß, *Crystalline Silicon Solar Cells*, John Wiley & Sons, Chichester, 1998, pp. 9–45; https://doi.org/10.1002/9781119033769.
16 X. Zhang, Q. Jiang, J. Wang and J. Tang, *Sol. Energy*, 2020, **206**, 670; https://doi.org/10.1016/j.solener.2020.06.007.
17 K. H. Park, S. Jung, J. Kim, B.-M. Ko, W.-G. Shim, S.-J. Hong and S. H. Song, *Nanomaterials*, 2021, **11**, 1464; https://doi.org/10.3390/nano11061464.
18 B. Ait Ali, R. Moubah, A. Boulezhar, S. Shi and H. Lassri, *Transactions on Electrical and Electronic Materials*, 2020, **21**, 436; https://doi.org/10.1007/s42341-020-00198-9.

*Received: 15th April 2024; Com. 24/7465*